

THEORETICAL MODELS AND BIOMATHEMATICAL ALGORITHMS FOR IDENTIFYING MULTIPLE GASTROINTESTINAL DIPOLES

Andrei Irimia^{1,2,3}, L. Alan Bradshaw^{1,2}, Jonathan D. Fouss³

¹ Living State Physics Laboratories
Department of Physics and Astronomy
Vanderbilt University
6301 Stevenson Science Center
Nashville, Tennessee, 37235, USA

² Biomagnetism Laboratory
Department of Physics and Astronomy
Vanderbilt University
6301 Stevenson Science Center
Nashville, Tennessee, 37235, USA

³ Department of Computing
and Information Systems
Lipscomb University
3901 Granny White Pike
Nashville, Tennessee, 37204, USA

Abstract

The study of the electrical gastric activity (EGA) is of great importance to the diagnosis of various pathological gastrointestinal (GI) conditions in humans. In order to analyze the characteristics of this phenomenon, a three-dimensional visualization of the current sources in the stomach was developed using magnetometer-recorded data of the gastric magnetic field as an input. An algorithm for solving the biomagnetic inverse problem was also developed that makes use of least-squares approximations in order to find the best-fitting current dipole orientations. Dipole locations were determined through the use of a recursive computational algorithm in which the forward biomagnetic model was employed. A theoretical biomathematical model was developed for this and adapted to take into account the anatomical configuration of the stomach and intestine, as well as other a priori criteria of investigation. The accuracy of the model developed was demonstrated using a simulation of magnetic fields in humans. In addition, various types of 3D simulations and visualizations were created in order to show the potential ability of the mathematical and computational tools created to accurately analyze anomalous biomagnetic field patterns.

Key Words: GI Modeling, Inverse Problem, Gastric Simulation.

1. GI Biomagnetism and Noninvasive Measurements

Many mathematical models of gastrointestinal (GI) biomagnetism often make heavy use of various signal-processing methods for identifying sources of electric current in the stomach and intestine based on magnetic field data recorded non-invasively using highly sensitive magnetometers, such as the Superconducting Quantum Interference Device (SQUID). These sources of electric current can be modeled as depolarization and repolarization current dipoles that are distributed as an isopotential ring of electrical control activity (ECA). The ECA manifests itself in the abdomen due to the presence

of coupled cells in the smooth muscle syncytium where transmembrane potentials produce dipole moments that vary in frequency and phase according to their anatomical position and configuration. These ECA variations in their own turn produce magnetic field variations, which can be recorded experimentally using SQUID magnetometers. Studies have shown that analyzing these magnetic field patterns can be a useful tool in detecting pathological states of the stomach in human patients, including gastroparesis and intestinal ischemia. It is therefore very important to have the ability of obtaining visual and numerical reconstructions of the magnetic fields produced in the abdomen since this may help us gain insight into the mathematical modeling of GI biomagnetic sources as well as into the biophysical phenomenology of gastric and intestinal diseases. The purpose of this article is to present a theoretical biomathematical model of the gastrointestinal magnetic field and to propose an efficient algorithm for reconstructing it using noninvasively recorded data from SQUID magnetometers. Given a data set containing experimentally recorded values of the magnetic field components B_x , B_y , and B_z , the process of determining the locations and orientations of the current dipoles that produce them involves solving the famous biomagnetic inverse problem. Specifically, the inverse problem refers to the identification of one or several current dipoles $\mathbf{Q}_1, \dots, \mathbf{Q}_n$ that account for the B_x , B_y , and B_z data recorded by the magnetometer. Solutions to the inverse problem are not unique due to the nature of Laplace's Equation and one method that is typically employed for obtaining a realistic solution consists of performing a least-squares approximation of the current dipole components $Q_{1x}, Q_{1y}, Q_{1z}, \dots, Q_{nx}, Q_{ny}, Q_{nz}$ that fit the recorded magnetic field values.

2. A Theoretical Model of the Biomagnetic Field

According to standard theoretical methods employed in biophysical modeling, a numerical reconstruction of the biomagnetic field \mathbf{B} can be obtained by making use of a quasi-static approximation to Maxwell's equations:

$$\mathbf{J} = \mathbf{J}_m + \sigma \mathbf{E} \quad (1)$$

$$\nabla \times \mathbf{B} = \mu_0 \mathbf{J} \quad (2)$$

$$\nabla \cdot \mathbf{B} = 0 \quad (3)$$

where \mathbf{E} is the electric field originating in the stomach, \mathbf{J}_m is the density of the source current, μ_0 is the magnetic permeability of free space and σ is the presumably constant conductivity of the conductor α in which the source of current is located. In our modeling case, α is represented by the stomach itself. Using these identities, the Law of Biot and Savart can be written in the alternative forms [1]:

$$\mathbf{B}(\mathbf{r}) = \mu_0 (4\pi)^{-1} \iiint_{\alpha} \mathbf{J}(\mathbf{r}_0) \times (\mathbf{r} - \mathbf{r}_0) |\mathbf{r} - \mathbf{r}_0|^{-3} d^3 \mathbf{r}_0 \quad (4)$$

$$\mathbf{B}(\mathbf{r}) = \mu_0 (4\pi)^{-1} \iiint_{\alpha} \nabla' \times \mathbf{J}(\mathbf{r}_0) |\mathbf{r} - \mathbf{r}_0| d^3 \mathbf{r}_0 \quad (5)$$

$$\mathbf{B}(\mathbf{r}) = \mu_0 (4\pi)^{-1} \iiint_{\alpha} \mathbf{J}_m(\mathbf{r}_0) \times (\mathbf{r} - \mathbf{r}_0) |\mathbf{r} - \mathbf{r}_0|^{-3} d^3 \mathbf{r}_0 \quad (6)$$

where \mathbf{r} represents the point in space for which \mathbf{B} is evaluated and \mathbf{r}_0 is the location of the current element due to which \mathbf{B} is produced at \mathbf{r} . In cases of gastrointestinal modeling, the magnetic field is present in the stomach due to a dipolar point source of moment \mathbf{Q} where

$$\mathbf{Q} = \iiint_{\alpha} \mathbf{J}_m(\mathbf{r}_0) d^3 \mathbf{r}_0 \quad (7)$$

In this case the current dipole models in fact a concentration of the impressed current in a single point \mathbf{r}_β :

$$\mathbf{Q} = \frac{\mathbf{J}_m(\mathbf{r})}{\delta(\mathbf{r} - \mathbf{r}_\beta)} \quad (8)$$

where δ represents the Dirac delta functional. Using the two formulas above, the Law of Biot and Savart can be rewritten as

$$\mathbf{B}(\mathbf{r}) \approx \mu_0 (4\pi)^{-1} \mathbf{Q} \times (\mathbf{r} - \mathbf{r}_0) |\mathbf{r} - \mathbf{r}_0|^{-3} \quad (9)$$

and the vector components of the magnetic field can be appropriately computed from the cross product above:

$$B_x \approx \mu_0 (4\pi)^{-1} |\mathbf{r} - \mathbf{r}_0|^{-3} [Q_y(z - z_0) - Q_z(y - y_0)] \quad (10)$$

$$B_y \approx \mu_0 (4\pi)^{-1} |\mathbf{r} - \mathbf{r}_0|^{-3} [Q_z(x - x_0) - Q_x(z - z_0)] \quad (11)$$

$$B_z \approx \mu_0 (4\pi)^{-1} |\mathbf{r} - \mathbf{r}_0|^{-3} [Q_x(y - y_0) - Q_y(x - x_0)] \quad (12)$$

In other words, the current dipole model can be used to approximate the value of the magnetic field by making the assumption that the current is concentrated at one point in space. In order to solve the inverse problem, knowledge of the forward problem is needed. The latter consists of determining the magnetic field \mathbf{B} given the electric potential \mathbf{V} and the current density \mathbf{J} . The inverse problem can thus be stated as the process of determining

\mathbf{V} and \mathbf{J} given \mathbf{B} . The mathematical model developed so far can be used for reaching this goal.

3. Data Acquisition and Signal Processing Considerations

For the purposes of this discussion, a typical experimental procedure for obtaining gastric biomagnetic field data involves the use of a Superconducting QUantum Interference Device (SQUID) magnetometer with 29 input channels that consist of magnetic pick-up coils positioned above the subject's abdominal region. Nineteen of the magnetometer's input locations are distributed above the stomach and intestine in the shape of two concentric, coplanar hexagons and programmed to record the B_z component of the magnetic field. Ten other such input channels are also positioned in the same plane as the other channels, five of each being used to record the B_x and B_y components of the magnetic field, respectively. An analog-to-digital device is then employed to convert the magnetic data recorded by these channels into binary file format. Magnetic field component values are stored in digital format in this file as a matrix with 29 columns—corresponding to each input channel of the SQUID magnetometer—and with a number of rows equal to the number of discrete sampling times at which magnetic field values are recorded. For the experimental data analyzed in this article, the sampling frequency used was 200 Hz. Input data was recorded for 86 seconds and the subject of the experiment was a rabbit. In the case of these animals, the electrical activity has a frequency of approximately 7 cycles per minute in the stomach and 20 cycles per minute in the intestine. In order to eliminate noise and to isolate both the stomach and intestine signal, two second-order, lowpass, digital Butterworth filters were separately applied to the experimental data set. The passbands w_s (for the stomach) and w_i (for the intestine) were chosen where

$$\frac{1}{60} \times 10^{-2} < w_s < \frac{7}{60} \times 10^{-2} \quad (13)$$

$$\frac{1}{60} \times 10^{-2} < w_i < \frac{20}{60} \times 10^{-2} \quad (14)$$

since each minute of data was assumed to contain seven full cycles of current dipole displacement for the stomach and twenty such cycles for the intestine. The multiplication factor of 10^{-2} was used because the filter was of second order and the sampling frequency for the experiment was 200 Hz. In addition to this type of filtering, linear detrending was used in order to eliminate polynomial time trends from the data.

4. Combinatorial Algorithms for Multiple Dipole Identification

The numerical reconstruction of the magnetic field described below makes use of a dense rectangular grid of

$n \times n$ points, where n is the number of input channels of the SQUID magnetometer—29 for this particular experimental example. The centroid of the grid was positioned at location $(x, y) = (0, 0)$ and the experimental values of the magnetic field \mathbf{B} were assumed to be sampled in the plane with equation $z = 0$. The point representing the center of the grid was thus $(x, y, z) = (0, 0, 0)$. The dimensions of the grid used for reconstructing the magnetic field were manipulated according to the experimental setup such that input channels located on the extremities of the input region were considered to be on the edges of the grid. In order to create a three-dimensional reconstruction of \mathbf{B} , a tetrahedron was created whose volume was positioned half above and half below the data sampling plane where $z = 0$. However, since magnetic field component data was not available for the entire grid, the method of Delaunay interpolation was used for the purposes of the algorithm described here in order to populate the entire grid with magnetic field values at the locations where these were not given by the experimental input points. Since the input area was in the shape of a hexagon and not a rectangle, additional interpolation had to be performed. For those regions situated outside the input perimeter, magnetic field component values were calculated according to a forward-difference derivative formula applied to the points located close to the edges of the perimeter.

The next phase of the computational process consisted of identifying the best-fitting locations of the current dipoles accounting for the experimental \mathbf{B} data. In the computational approach adopted, possible dipole locations were assumed to be located within a cylinder whose horizontal cross-section was centered at $(0, 0)$ and where the stomach dipoles can be located anatomically. Instead of performing a complete search within the reconstruction volume, dipole positions were determined by applying recursive projections of the forward model at statistically determined positions on the original grid until the best fitting dipoles \mathbf{Q}_1 and \mathbf{Q}_2 were found. The degenerate recursive case consisted of the degree of accuracy specified for computing the centroids and the magnetic field values due to dipoles located at these centroids. In other words, dividing best-fitting sectors into smaller ones ended based on the level of grid refinement specified in the program. The vector components of the two dipoles were determined through the use of a least-squares approximation whose fitting criterion was based on a restricted, anatomically relevant area of the body. The cylinder under consideration—within which current dipoles were assumed to be positioned—was thus divided into eight sectors of equal area and symmetric with respect to the x and y axes, where the initial position of each dipole was computed. The assumed initial positions of the dipoles were calculated for each of these sectors from the centroid formulas

$$\bar{x}_n = \frac{\int_{a_n}^{b_n} x\sqrt{1-x^2} dx}{\int_{a_n}^{b_n} \sqrt{1-x^2} dx} \quad (15)$$

$$\bar{y}_n = \frac{\left(\frac{1}{2}\right) \int_{a_n}^{b_n} (1-x^2) dx}{\int_{a_n}^{b_n} \sqrt{1-x^2} dx} \quad (16)$$

where \bar{x}_n and \bar{y}_n represent the centroid coordinates of the n -th sector and a and b represent the x -coordinate limits of the n -th sector where $a < b$. These two values are thus to be determined successively as the left and right extremities of each sector according to how the grid is sliced. After identifying the best-fitting region, further estimates of the dipole locations are made recursively until the best fit in a least squares sense is found at one of these locations.

In order to find the best vector components of the dipole \mathbf{Q} , the method of least squares approximation was used where the analytical form of the function describing the magnetic field—as in Eq. (10), (11), (12)—was found with the use of the Biot-Savart law. This procedure involved a minimization of the partial derivatives for these three functions with respect to the four variables representing each of the dipole components. Since the experimental data was collected above the entire abdomen, magnetic field values were assumed to be affected not only by the presence of the stomach, but also by that of the intestine. The circle containing possible dipole locations was therefore split into an upper half—containing a dipole accounting for the stomach signal—and a lower half—containing a second dipole accounting for the intestine signal. In other words, the function describing the total magnetic field \mathbf{B} at any point was considered to be the sum of two other functions, i.e.,

$$\mathbf{B} = \hat{\mathbf{B}} + \check{\mathbf{B}} \quad (17)$$

where $\hat{\mathbf{B}}$ corresponds to the function describing the magnetic field of the stomach and $\check{\mathbf{B}}$ to that of the intestine, i.e.,

$$\hat{\mathbf{B}}_x \approx \mu_0(4\pi)^{-1} |\mathbf{r} - \hat{\mathbf{r}}_0|^{-3} \left[\hat{Q}_y(z - \hat{z}_0) - \hat{Q}_z(y - \hat{y}_0) \right] \quad (18)$$

$$\check{\mathbf{B}}_x \approx \mu_0(4\pi)^{-1} |\mathbf{r} - \check{\mathbf{r}}_0|^{-3} \left[\check{Q}_y(z - \check{z}_0) - \check{Q}_z(y - \check{y}_0) \right] \quad (19)$$

where $\hat{\mathbf{r}}_0 = (\hat{x}_0, \hat{y}_0, \hat{z}_0)$ is the location of the stomach dipole and $\check{\mathbf{r}}_0 = (\check{x}_0, \check{y}_0, \check{z}_0)$ is the location of the intestine dipole. As can be seen from the formulas above, $\hat{\mathbf{B}}$ and $\check{\mathbf{B}}$ are functions of three variables, \hat{Q}_x , \hat{Q}_y , \hat{Q}_z and \check{Q}_x , \check{Q}_y , \check{Q}_z , respectively from the perspective of least-squares

approximations. The former three are the coordinates of the stomach dipole and the latter three are the coordinates of the intestine dipole. These are considered variables for the approximation because minimization of the squared errors is performed with respect to them. The sum of the two functions accounts for the entire value of the magnetic field at any point in space. The natural approach is to assume that the magnetic field function can be approximated by the function derived above for each of its individual vector components, in which case the values of \hat{Q}_x , \hat{Q}_y , and \hat{Q}_z —for the stomach dipole—and \bar{Q}_x , \bar{Q}_y , and \bar{Q}_z —for the intestine dipole—need to be computed. Since the approximation can be made in order to minimize errors in the value of the magnetic field component B_z , the four parameters with respect to which minimization is performed are \hat{Q}_x , \hat{Q}_y , \bar{Q}_x , and \bar{Q}_y as follows:

$$\frac{\partial}{\partial Q_x} \Lambda = \sum_{i=1}^m \sum_{j=1}^n 2(\tilde{B}_z^{ij} - \hat{B}_z^{ij} - \bar{B}_z^{ij}) \left[-\frac{\mu_0 (\hat{y}_{ij} - \hat{y}_0)}{4\pi |\mathbf{r}_{ij} - \hat{\mathbf{r}}_0|} \right] = 0 \quad (20)$$

$$\frac{\partial}{\partial Q_y} \Lambda = \sum_{i=1}^m \sum_{j=1}^n 2(\tilde{B}_z^{ij} - \hat{B}_z^{ij} - \bar{B}_z^{ij}) \left[\frac{\mu_0 (\hat{x}_{ij} - \hat{x}_0)}{4\pi |\mathbf{r}_{ij} - \hat{\mathbf{r}}_0|} \right] = 0 \quad (21)$$

$$\frac{\partial}{\partial Q_x} \Lambda = \sum_{i=1}^m \sum_{j=1}^n 2(\tilde{B}_z^{ij} - \hat{B}_z^{ij} - \bar{B}_z^{ij}) \left[-\frac{\mu_0 (\bar{y}_{ij} - \bar{y}_0)}{4\pi |\mathbf{r}_{ij} - \bar{\mathbf{r}}_0|} \right] = 0 \quad (22)$$

$$\frac{\partial}{\partial Q_y} \Lambda = \sum_{i=1}^m \sum_{j=1}^n 2(\tilde{B}_z^{ij} - \hat{B}_z^{ij} - \bar{B}_z^{ij}) \left[\frac{\mu_0 (\bar{x}_{ij} - \bar{x}_0)}{4\pi |\mathbf{r}_{ij} - \bar{\mathbf{r}}_0|} \right] = 0 \quad (23)$$

where Λ is the sum of squared errors over the $n \times m$ channel input points grid. \tilde{B}_z^{ij} is the experimental value of \mathbf{B} as measured by the SQUID magnetometer and \hat{B}_z^{ij} , \bar{B}_z^{ij} are the computed value for the z magnetic field component produced by the stomach and intestine dipoles, respectively. The choice for B_z as the vector component function used for the minimization is only due here to the fact that more input channels were available for this component of \mathbf{B} . The data for other components of the magnetic field can be used successfully if deemed necessary, according to the experimental setup. The superscripts i and j used above indicate the grid subscripts at which the magnetic field values are evaluated. For a polynomial of n -th degree used to fit a set of experimental data, Λ would be

$$\Lambda = \sum_{i=1}^n (Y_i - a_0 - a_1 x_1 - a_2 x_2 - \dots - a_n x_i^n)^2 \quad (24)$$

which indicates that for our purposes the summation term Y_i becomes \tilde{B}_z^{ij} and the n -th degree polynomial in one dimension becomes $(\tilde{B}_z^{ij} + \hat{B}_z^{ij})$, which would represent the

computed function for the magnetic field in two dimensions. Thus,

$$\Lambda = \sum_{i=1}^m \sum_{j=1}^n (\tilde{B}_z^{ij} - \hat{B}_z^{ij} - \bar{B}_z^{ij})^2 \quad (25)$$

where we can add the magnetic field values due to the stomach dipole to the value due to the intestine dipole because the total magnetic field at any point in space is the sum of the two according to vector addition rules. In all the formulas below, $|\mathbf{r}_i - \mathbf{r}_0|$ is the vector magnitude of $(\mathbf{r}_i - \mathbf{r}_0)$ in Cartesian coordinates, which can be found according to the formula

$$|\mathbf{r}_i - \mathbf{r}_0| = \sqrt{\sqrt{(x - x_0)^2} + \sqrt{(y - y_0)^2} + \sqrt{(z - z_0)^2}} \quad (26)$$

The matrix that can be used for performing the least-squares minimization of the partial derivatives of Λ with respect to each of the dipole components becomes

$$\boldsymbol{\eta} = (\boldsymbol{\eta}_1 \quad \boldsymbol{\eta}_2 \quad \boldsymbol{\eta}_3 \quad \boldsymbol{\eta}_4 \quad \boldsymbol{\eta}_5)^T \quad (27)$$

where each of the rows in $\boldsymbol{\eta}$ is equal to a rearranged and simplified equation resulting from minimizing the partial derivatives shown above, i.e.,

$$\boldsymbol{\eta}_1 = \begin{pmatrix} \hat{Q}_x \sum_{i=1}^m \sum_{j=1}^n \frac{(y_{ij} - \hat{y}_0)^2}{|\hat{\mathbf{r}}_{ij} - \hat{\mathbf{r}}_0|^6} \\ -\hat{Q}_y \sum_{i=1}^m \sum_{j=1}^n \frac{(x_{ij} - \hat{x}_0)(y_{ij} - \hat{y}_0)}{|\hat{\mathbf{r}}_{ij} - \hat{\mathbf{r}}_0|^6} \\ \bar{Q}_x \sum_{i=1}^m \sum_{j=1}^n \frac{(y_{ij} - \hat{y}_0)(y_{ij} - \bar{y}_0)}{|\hat{\mathbf{r}}_{ij} - \hat{\mathbf{r}}_0|^3 |\bar{\mathbf{r}}_{ij} - \bar{\mathbf{r}}_0|^3} \\ -\bar{Q}_y \sum_{i=1}^m \sum_{j=1}^n \frac{(y_{ij} - \hat{y}_0)(x_{ij} - \bar{x}_0)}{|\hat{\mathbf{r}}_{ij} - \hat{\mathbf{r}}_0|^3 |\bar{\mathbf{r}}_{ij} - \bar{\mathbf{r}}_0|^3} \\ \frac{4\pi}{\mu_0} \sum_{i=1}^m \sum_{j=1}^n \frac{(y_{ij} - \hat{y}_0)}{|\hat{\mathbf{r}}_{ij} - \hat{\mathbf{r}}_0|^3} B_z^{ij} \end{pmatrix}^T \quad (28)$$

where x_{ij} , y_{ij} , refer to the x and y coordinates of the i -th and j -th point on the grid taken under the double summation and $\hat{\mathbf{r}}_{ij}$ refers to the vector extending from the origin to the point determined by (x_{ij}, y_{ij}) . In the matrix column above, \hat{x}_0 , \hat{y}_0 are the x and y coordinates of the stomach dipole located at $\hat{\mathbf{r}}_0$ whose vector components are $(\hat{Q}_x, \hat{Q}_y, \hat{Q}_z)$. Similarly, \bar{x}_0 , \bar{y}_0 are the x and y coordinates of the stomach dipole located at $\bar{\mathbf{r}}_0$ with vector components $(\bar{Q}_x, \bar{Q}_y, \bar{Q}_z)$. This set of normal equations as described above can be simultaneously

solved using, for example, the Gauss-Jordan algorithm for matrix reduction. The only other vector components that are needed for the two dipoles are \hat{Q}_z and \bar{Q}_z , which can be evaluated by applying the same approximation method to minimize the squared errors for another vector component of \mathbf{B} , e.g. B_x . The computation can be performed by following the same method described

above. In order to improve the magnetic field calculation, current dipoles were sequentially added one by one. Their magnitudes and orientations were computed in order to fit the residuals of the previous dipoles computed. The process was repeated until the sum of these residuals converged to zero or to a minimum value after which the following sum in this sequence diverged. For most of the

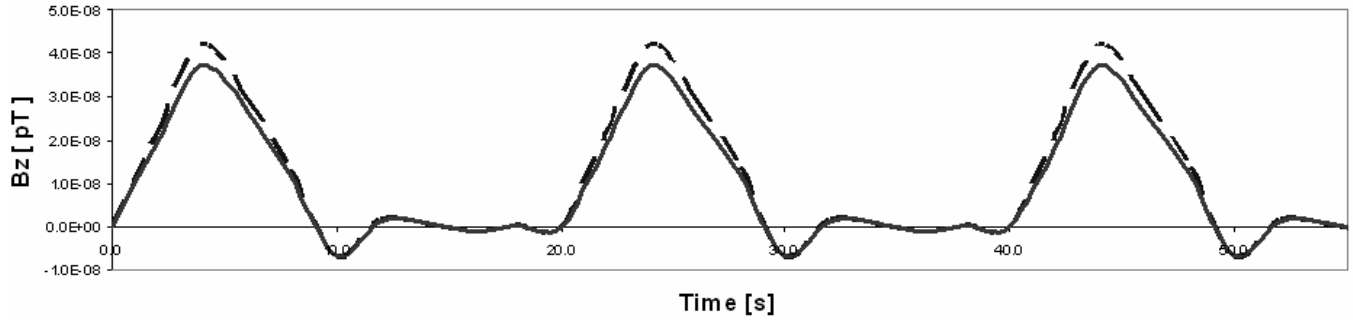


Figure 1. Simulated and reconstructed values of B_z for a sample simulated signal of a SQUID input channel. Simulated values are shown by the dotted line while reconstructed values are shown by the continuous one. Program runs yielded an average accuracy of approximately 96 % in the computed values of the magnetic field vector B_z . The program was tested using values from 6 channels located above the abdomen.

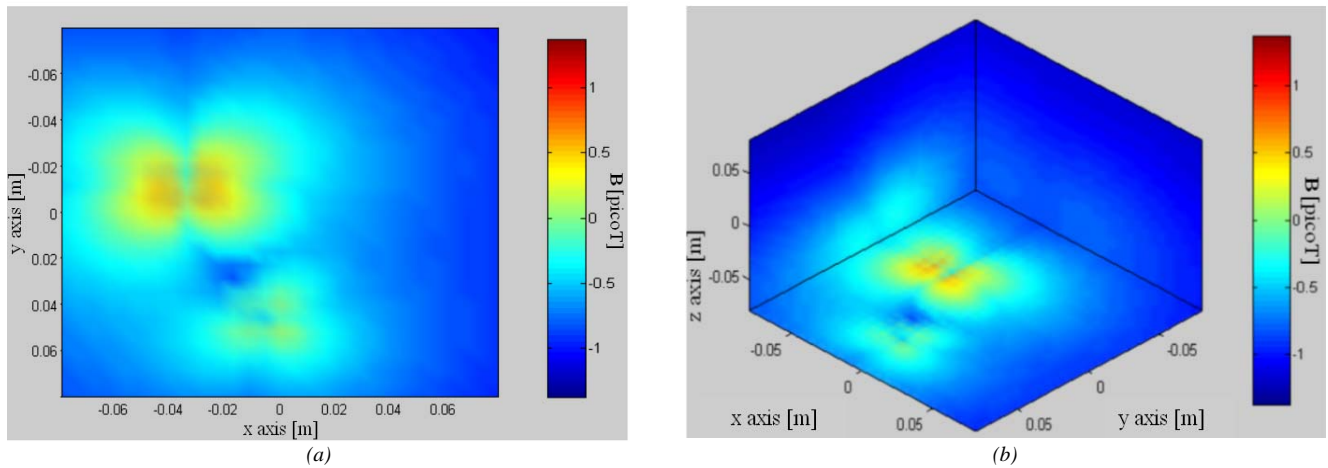


Figure 2. Visualization of the magnetic field magnitudes in the rabbit abdomen. Dipole locations, orientations and magnitudes are identical to the ones in Figure 5. The stronger dipole is located in the stomach, as shown above. The magnitude of the field is highest at the level of the intestine and then decreases sharply in the direction of the positive z axis, above the abdomen and outside the rabbit body. In (a), the tetrahedron is viewed from directly below (azimuth = 0° , elevation = -90°). In (b), the perspective point is located to the right side and below the measurement plane (azimuth = 45° , elevation = -45°).

data studied, however, the single dipole model was found to be sufficiently accurate for the purposes of the simulations and no additional dipoles had to be added.

The computational model ($\hat{\mathbf{B}}$) was thus calculated and compared to the experimental data set ($\bar{\mathbf{B}}$) with an average accuracy of approximately 90% due to noise and computational inaccuracies. The model was adjusted so that the dipole search would yield realistic positions of low depth due to the fact that many deep dipoles tend to be unrealistic and of little importance to the overall model (cf. [5], [16], [20], [21]). In addition to these specifications, the grid section in which dipole searches were carried out was sensibly reduced so as to exclude peripheral input points. This ensured that the regions of

maximum interest in terms of gastric biomagnetic activity were given appropriate attention. Furthermore, by including this information into the program, considerable searching time was saved and dramatic computational improvements were made possible. Guidelines for including a priori information that are similar to those presented here can also be found in [3], [4], and [7].

5. Computation and Visualization Results

In order to demonstrate the accuracy of the computational model developed, an algorithm was developed for it and implemented using a MATLAB® program. The input to this program consisted of data in binary format collected from a rabbit using a SQUID magnetometer, as described

above. In order to obtain a visual assessment of the reconstruction's accuracy, experimental and computational values for B_z were plotted for a set of six SQUID input channels located above the abdomen. Input data was decimated by a factor of 33 experimental frames to one reconstructed frame, which implies that the field was reconstructed only for one in every 33 frames from the experimental data file. For a majority of the reconstruction frames, average errors of 10.5% the original biomagnetic field values were obtained. These are due to the noise affecting the experimental values, as well as to computational inaccuracies resulting from the nature of the approximation, i.e. the estimation of a surface based on a finite number of two-dimensional grid points. As a method of testing the reconstruction accuracy of the algorithm developed, a number of SQUID input channels were selected for which the experimental and the computational values of the B_z vector component were plotted as functions of time over a period of 50 s. One such plot is displayed in Figure 1, where the time evolution of B_z is shown for a simulated signal of a SQUID channel located above the stomach. As one can notice from the figure, the percentage of accuracy of the computational value for B_z with respect to the original experimental value is above 90% for most of the data time sequence analyzed. For the entire 86 seconds sampled, the average error was found to be 10.5%.

One useful method of visualizing the results of the reconstruction consists of creating graphs for the values of the magnetic field vector components B_x , B_y , and B_z in the plane $z = 0$, corresponding to the level above the abdomen where the SQUID magnetometer was positioned. Images of the biomagnetic field magnitude $|\mathbf{B}|$ were created using the same principle as above where the vector magnitude

$$|\mathbf{B}| = \left[(B_x)^2 + (B_y)^2 + (B_z)^2 \right]^{1/2} \quad (29)$$

was used for plotting purposes, as in Figure 2. From the two images in this figure, the signal due to the intestine appears to be stronger than that from the stomach and to be localized in the upper part of the organ.

6. Conclusion

The mathematical method of analysis that has been developed for analyzing the biomagnetic field of the stomach and intestine is a promising procedure for the identification of pathological states in humans. This may open new horizons to the field of medical gastrointestinal research and useful results are expectable in this area of scientific interest due to the development of this procedure. The demonstrated accuracy of the simulation

and of the inverse problem algorithm that has been concurrently designed are encouraging for the state of this art as well as for the theoretical modeling and exploration of the intrinsically complex mechanisms at work within the organs of the human body.

7. Acknowledgements

The author wishes to thank reviewers of the manuscripts for their insightful remarks concerning the theoretical and computational aspects of this endeavor. Research funding was provided by the Living State Physics Laboratories at Vanderbilt University through the Veterans' Affairs Research Service, Grant NIH R01 DK58697-01. Travel expenses were covered by the College of Natural and Applied Sciences at Lipscomb University.

References

- [1]. J. Sarvas, Basic mathematical and electromagnetic concepts of the biomagnetic inverse problem, *Physics in Medicine and Biology*, 32 (1), 1987, 11-22.
- [2]. S. Baillet, J. C. Mosher, R. M. Leahy, Electromagnetic brain mapping, *IEEE Signal Processing Magazine* 18 (6), 2001, 14-20.
- [3]. R. P. Grasman, H. M. Huzenga, L. W. Waldorp, Maximum likelihood spatiotemporal EEG/MEG source analysis. *Proc. 12th International Conference on Biomagnetism*, Helsinki Institute of Technology, Helsinki, Finland, 2000.
- [4]. Kaneko, M., Okabe, Y., Sekine, F., Inverse analysis of biomagnetic fields in consideration of the external magnetic noise. *Proc. 12th International Conference on Biomagnetism*, Helsinki Institute of Technology, Helsinki, Finland, 2000.
- [5]. Kuriki, S., Shirai, N., Takeuki, F., Multidipole analysis using a modified parameter search method. *Proc. 12th International Conference on Biomagnetism*, Helsinki Institute of Technology, Helsinki, Finland, 2000.
- [6]. Baillet, S., Garnero, L., A Bayesian Approach to Introducing Anatomic-Functional Priors in the EEG/MEG Inverse Problem. *IEEE Transactions on Biomedical Engineering* 44 (5), 1997, 374-385.
- [7]. Baillet, S., Mosher, J. C., Jerbi, K., Leahy, R. M., Hybrid MEG source characterization by cortical remapping and imaging of parametric source models. *Proc. 12th International Conference on Biomagnetism*, Helsinki Institute of Technology, Helsinki, Finland, 2000.
- [8]. Baillet S., Garnero, L., Gavit L., Mangin, J. F., Pescatore, J., Multiresolution Bayesian approach for brain electrical tomography: application to reconstructing the cortical representation of hand from MEG data. *Proc. 12th International Conference on Biomagnetism*, Helsinki Institute of Technology, Helsinki, Finland, 2000.